PROCEEDINGS, 51st Workshop on Geothermal Reservoir Engineering
Stanford University, Stanford, California, February 9-11, 2026
SGP-TR-230

Estimating Thermal Breakthrough at Utah-FORGE from a Thermo-Hydraulic Fracture Model Calibrated to Circulation Data

Lynn MUNDAY*[1], Bozo VAZIC[1], Cornelius OTCHERE[1,2], Aleta FINNILA[3], Som DHULIPALA[1], Robert PODGORNEY[1]

[1]Idaho National Laboratory, Idaho Falls, Idaho, U.S.A.
[2]Johns Hopkins, Baltimore, Maryland, U.S.A.
[3]WSP USA, Redmond, Washington, U.S.A.
*lynn.munday@inl.gov

Keywords: Enhanced geothermal systems, native state, FORGE

ABSTRACT

The Utah Frontier Observatory for Research in Geothermal Energy (FORGE) conducted a 30-day commercial-scale circulation test in August 2024 between wells 16A(78)-32 and 16B(78)-32. During this test, field data were collected, including injection pressure, spinner log measurements of mass flow near each injection perforation, tracer injection and recovery, and mass injection and recovery rates. A discrete fracture network (DFN) of the FORGE site was developed using microseismic data from hydraulic stimulation and circulation tests, core samples, strain gauge measurements, and inferred fracture connectivity derived from flow and pressure responses. In this study, a multi-component thermal-hydraulic simulation of the DFN was calibrated to match the observed field data and used to predict thermal breakthrough behavior. The DFN is modeled as a set of 2D fractures embedded in a 3D domain, with fracture permeabilities dependent on their aperture and flow rate. A linear relationship between mass flow rate and fracture aperture calibrated to the circulation test data is used to parameterize the DFNs based on spinner log data. Using the calibrated parameters, thermal-hydraulic simulations were performed to model a 180-day circulation test and estimate the time to thermal breakthrough.

1. INTRODUCTION

Enhanced geothermal systems (EGS) offer firm, carbon-free power by extracting heat from low-permeability hot rock using engineered fracture networks. To accelerate EGS technology development and reduce the risks associated with field-scale demonstrations, the U.S. Department of Energy Office of Geothermal established the Frontier Observatory for Research in Geothermal Energy (FORGE) as a dedicated field laboratory near Milford, Utah. The Utah FORGE program has progressed through site selection, site characterization, and full implementation/operations with extensive data acquisition and open dissemination through the Geothermal Data Repository (Moore et al., 2019).

In 2024, Utah FORGE conducted an extended circulation test between wells 16A(78)-32 (injector) and 16B(78)-32 (producer) that included zonal injection pressure measurements, spinner logs to quantify flow partitioning among perforation clusters, and tracer injection and recovery (McLennan et al., 2024; Hartvig et al., 2025). These datasets provide a rare opportunity to constrain reservoir-scale models against multiple observables and to evaluate how fracture-network connectivity controls both hydraulic impedance and thermal drawdown.

In this paper, we present coupled thermo-hydraulic DFN simulations of the Utah FORGE August 2024 circulation test using the finite-element reservoir simulator FALCON built on the MOOSE framework (Giudicelli et al., 2024; Podgorney et al., 2021). Building on prior calibration using multi-objective Bayesian optimization (Otchere et al., 2026), we apply a flow-rate–dependent aperture relationship across the full DFN model and compare simulation outputs with field measurements of injection pressure, far-field pressure, production rate, tracer recovery, and production temperature from the August 2024 circulation test. We then extend simulations to 180 days to estimate the onset and rate of thermal drawdown, providing guidance for future long-duration FORGE experiments. For the scope of this conference paper we focus on (i) DFN thermo-hydraulic modeling assumptions, (ii) calibration logic tied directly to the August–September 2024 circulation observations, and (iii) a 180-day projection of production temperature response.

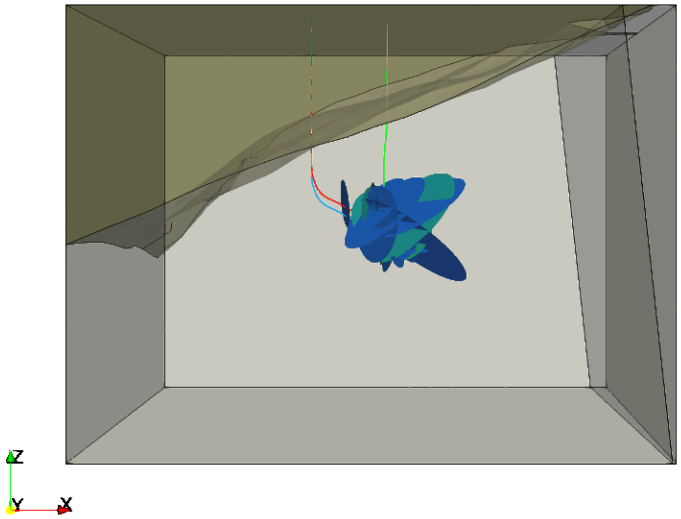

Figure 1: Simulation domain including DFN, surrounded by granite and sediment. Opal mountain fault is shown by the title plane on the right.

2. THERMO-HYDRO-MECHANICAL FIELD EQUATIONS

We model coupled fluid flow, tracer transport, and heat transfer in a DFN embedded in a 3D host rock domain (Figure 1) using FALCON/MOOSE (Giudicelli et al., 2024; Wilkins et al., 2021; Podgorney et al., 2021). The formulation solves (i) single-phase water mass conservation with Darcy flow in fractures and matrix, (ii) advection–dispersion transport of an inert aqueous tracer, and (iii) an energy balance with conductive heat exchange between rock and circulating fluid. Injection and production are represented as point source/sink terms at fracture–well intersections; zonal injection allocation follows the August 2024 spinner log distribution for well 16A(78)-32, and production is applied at well 16B(78)-32 intersections. The fluid is injected into each fracture at 323K (50C). Fluid properties are evaluated as functions of pressure and temperature using standard water property correlations; numerical stabilization uses fully upwind treatment for advective terms. Boundary conditions apply prescribed temperature (and top-surface pressure) consistent with the FORGE native-state model (Liu, et al. 2022), with lateral flux-matching conditions to approximate a semi-infinite far field. More information about the governing equation being solved and material properties being used can be found in Otchere et al., (2026) and Wilkins et al., (2021).

3. FRACTURE AND MATRIX MATERIAL MODELS

The domain in Figure 1 is simplified by excluding the sediment layer and the Opal Mountain fault, leaving only granite and discrete fractures in the simulation domain. While metamorphic gneiss is also present in the reservoir, the lithologic boundaries between the granite and gneiss units are not yet known and the material properties of the two lithologies appear to be similar (e.g. Young's Modulus, Poisson's ratio, etc. as measured from sonic logs) (Jones, 2025). Constant matrix permeability and porosity are used for the granite. Fractures are modeled as two-dimensional elements embedded within a three-dimensional matrix. To account for the lower-dimensional representation, fracture permeability and porosity are scaled by the fracture aperture giving effective properties. The effective fracture permeability follows a Kozeny–Carman-type cubic-aperture relationship given by

$$k = r\frac{a^3}{12}, \tag{6}$$

with the aperture, a, given by the following linear function for pore pressure

$$a = a_0 + \frac{1}{K}(p - p_0), \tag{7}$$

where K is the bulk modulus and a_0 is the reference aperture at the reference pressure. The fracture is assumed to be fully saturated, making the porosity unity and the effective porosity equal to the aperture, $\phi = a$.

Values for the initial fracture aperture and granite properties are taken from our previous work (Otchere, 2026) where we used multi-objective Bayesian optimization to determine granite and fracture properties for a small subset of simplified fractures that best match the August 2024 circulation data for injection pressure, mass production and tracer production (McLennan, 2024, Hartvig et al. 2025). The zone 10 fracture and surrounding granite were parameterized with a spatially variable aperture with preferential flow between the injection and production points to accommodate its high flow rate of 2.58 barrels per minute (bpm). The other fractures, with flowrates below 1

bpm, were parameterized with a constant initial aperture to fit the injection pressure shown by the points in Figure 2 and fit with a linear equation (Otchere et al., 2026). We use this linear fit to determine the initial fracture aperture based on the injection rate for all fractures except those in zone 10. See Otchere et al. (2026) for more information on the material properties and fitting used in this work.

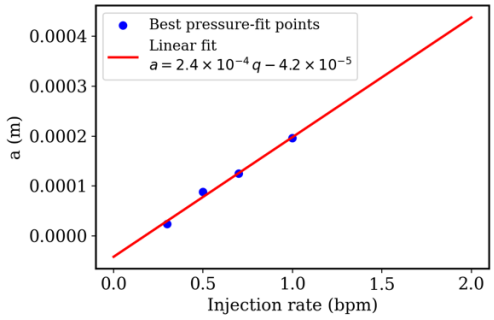

Figure 2: Calibrated fracture aperture versus injection rate derived parameters. The red line is the linear fit used in this work (Otchere et al., 2026).

4. DISCRETE FRACTURE NETWORK

The discrete fracture network (DFN) utilized in this study is based on the version released on GDR in July 2025 (Finnila 2025, Finnila 2026). The DFN contains 131 fractures divided across 10 injection zones. The DFN is divided into clusters that provide connectivity between each injection zone and the production well. The flow rate into each cluster zone is provided by the spinner log data from the August 2024 circulation test. The initial cluster aperture is determined using the cluster flow rates with the linear fit in Figure 2. The DFN with fractures colored by their initial apertures are shown in Figure 3. The fracture clusters are filtered in Figure 3 to show those fractures with the largest apertures and therefore the largest flow rates. The slices of the DFN in the right column of Figure 3 illustrate the fracture clusters connecting the injection and production wells. These filtered clusters visually represent which fractures in the DFN receive the most flow, along with their orientation and size.

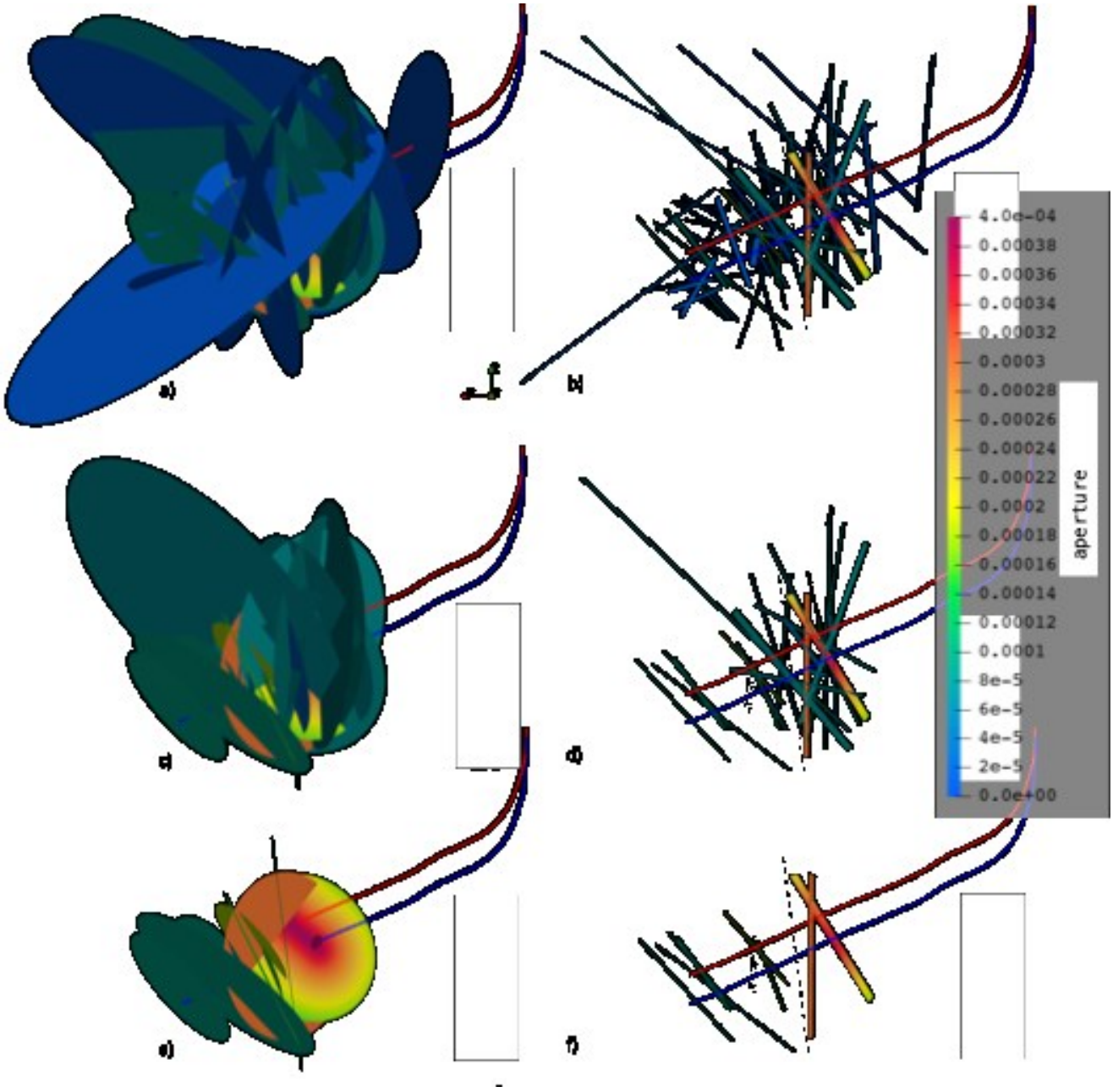

Figure 3: DFN colored by initial aperture at reference pressure. The left column displays the full extent of the fracture network, while the right column focuses on a 15-meter section surrounding the injection and production wells. The top row (images a and b) presents the complete DFN. The middle row (images c and d) highlights fractures with apertures greater than 0.01 mm. The bottom row (images e and f) features fractures with apertures exceeding 0.085 mm.

5. SIMULATION RESULTS

This section compares FORGE reservoir simulation outputs to the August–September 2024 extended circulation test data and summarizes the model's implications for longer-term performance. In Section 5.1 we compare injection-zone pressures in well 16A-32, far-field pressure at monitoring well 58-32, mass recovery, and tracer recovery from in well 16B-32 (McLennan et al., 2024, Hartvig et al., 2025). In Section 5.2 we post-process the simulated downhole production conditions in well 16B-32 using a 1D wellbore heat-transfer model to obtain wellhead temperatures comparable to surface measurements (McLennan et al., 2024).

5.1 Thermo-Hydraulic Reservoir Simulation

Figure 4 compares the simulated and observed injection pressures for each perforation cluster in well 16A(78)-32, with each curve colored by the measured mass injection ratio. For the highest-flow clusters, the model reproduces the magnitude and early-time evolution of injection pressure during the first ~15 days, suggesting that the calibrated fracture impedance and near-wellbore connectivity are reasonable. After approximately day 15, the measured wellhead pressure declines while the simulated pressure remains elevated. This

misfit likely reflects time-dependent processes not represented in the present thermo-hydraulic model (e.g., evolving fracture conductivity or redistribution of flow among sub-perforations).

The pressure response at monitoring well 58-32 (Figure 5) is reproduced over the 30-day test, indicating that the bulk storage/compressibility and boundary-condition representation of the larger-scale domain are consistent with the observed far-field hydraulic diffusion. The simulated production mass rate (Figure 6) underpredicts the observed recovery and stabilizes at ~80% recovery over 180 days, suggesting that overall connectivity and/or effective transmissivity between injection and production are slightly underestimated by the current DFN parameterization. The simulation captures the main peak in tracer recovery (Figure 7), which is controlled by the dominant flow path associated with the highest-flow fracture in Zone 10 (Otchere et al., 2026; Hartvig et al., 2025). The post-peak divergence in tracer recovery indicates that the model likely overestimates late-time exchange with lower-flow fractures and/or dispersion in secondary pathways.

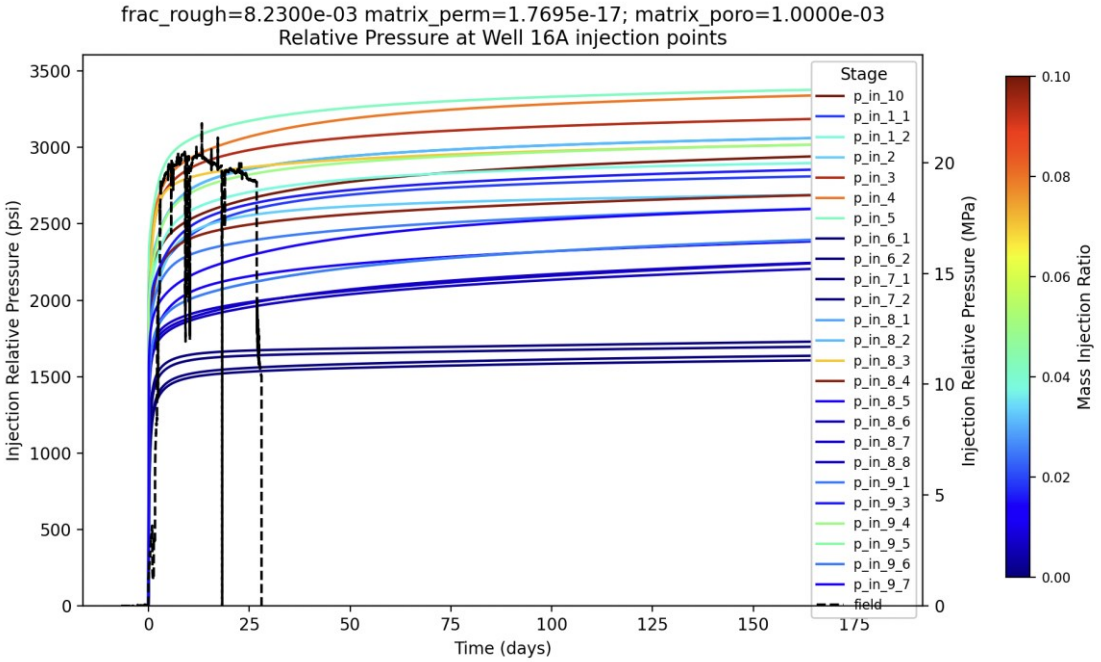

Figure 4: Injection pressure at each zone in well 16A(78)-32 colored by mass injection ratio (multiply by 10 to get bpm) compared to well head field data in black.

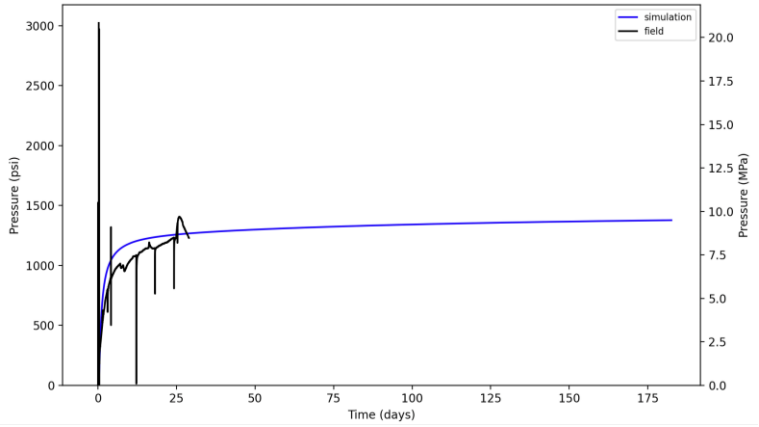

Figure 5: Fluid pressure in well 58-32 for simulated (blue) and field data (black).

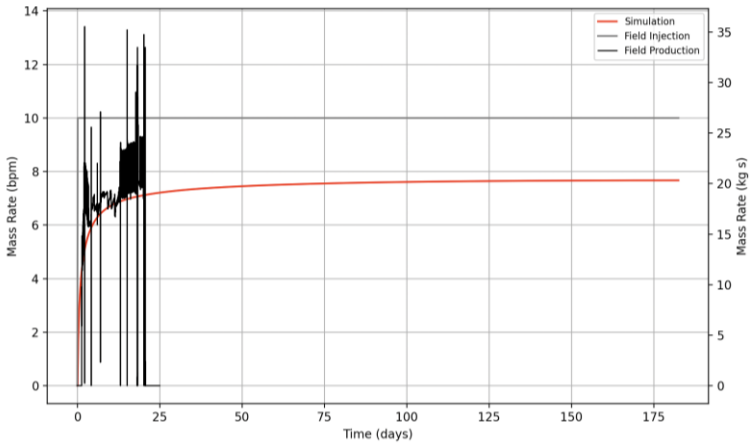

Figure 6: Mass production from well 16B(78)-32 showing simulation (red) and field data (black). Injection rate of 10 bpm into well 16A(78)-32 shown by grey line.

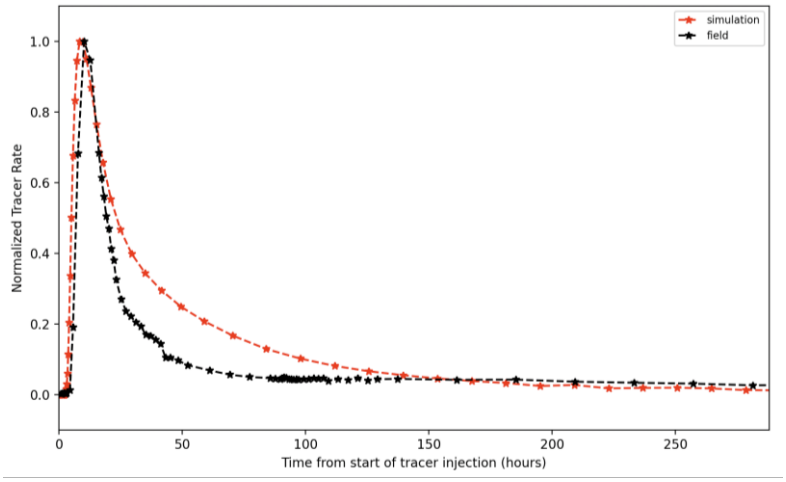

Figure 7: Tracer recovery from well 16B(78)-32 showing simulation (red) and field data (black) accounting for fluid travel time down well 16A-32 and back up well 16B-32.

5.2 Thermo-Hydraulic Well Model

The reservoir simulation provides the time histories of produced mass flow rate and fluid temperature at the fracture–well intersections in well 16B(78)-32. As a post-processing step, we propagate this production fluid to the surface using a 1D thermo-hydraulic wellbore model that accounts for advective transport in the pipe and heat exchange with the surrounding formation. This isolates near-wellbore thermal losses so simulated surface temperatures can be compared directly to the circulation-test measurements.

Figure 8 shows the simulated production temperature as a function of time at several depths, including the fracture zone and the wellhead. The fluid temperature at the fracture intersection rises rapidly as injected water begins to sweep the highest-transmissivity flow paths and reaches a maximum after ~35 days; at the surface, the peak is delayed to ~70 days due to wellbore heat exchange. The resulting wellhead temperature matches the observed circulation-test trend over the first 30 days (Figure 9), supporting the combined DFN + wellbore model. When extended to 180 days, the simulation predicts the onset of gradual thermal drawdown at the wellhead after ~100 days, with an approximately constant cooling rate of 0.032 K/day (Figure 10). Over the final 80 days of the 180-day forecast, this corresponds to ~2.6 K of cooling relative to the peak temperature, indicating that thermal breakthrough is beginning but remains modest for the simulated injection strategy.

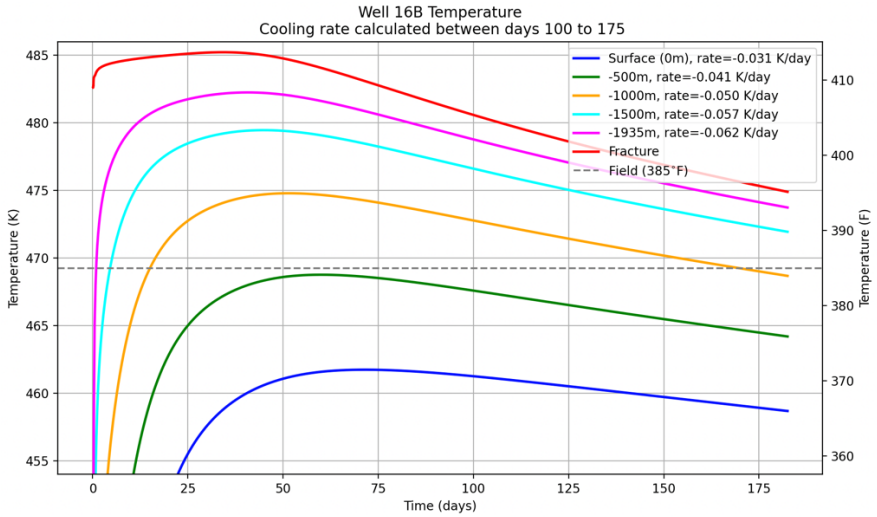

Figure 8: Temperature history in well 16B(78)-32 as a function of well depth.

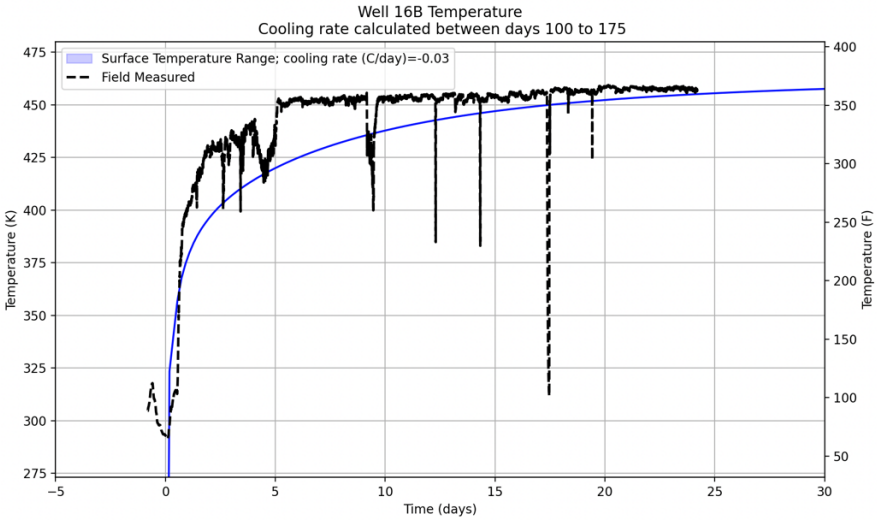

Figure 9: Surface temperature for well 16B(78)-32 showing simulation (blue) and field data (black).

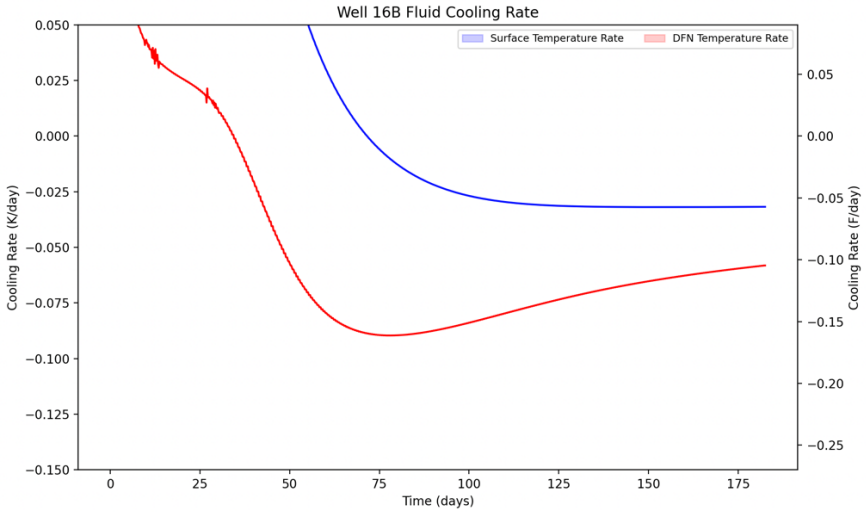

Figure 10: Rate of temperature change in 16B(78)-32 at the fractures (red) and at the surface (blue).

6 CONCLUSION

We calibrated a thermo-hydraulic reservoir model containing DFNs of Utah FORGE to match key observations from the August–September 2024 circulation test, including injection pressure response, mass recovery, and tracer recovery. Using the calibrated aperture–injection-rate relationship to initialize the full DFN, 180-day simulations predict that production temperatures begin a sustained decline after ~100 days of continuous circulation at 10 bpm in this configuration. Remaining mismatches at late time (pressure reduction and post-peak tracer recovery) indicate that additional processes—e.g., evolving fracture conductivity or unmodeled connectivity—may influence long-term behavior and will be addressed in a full journal submission.

ACKNOWLEDGEMNT

Funding for this work was provided by the U.S. DOE under grant DE-EE0007080 “Enhanced Geothermal System Concept Testing and Development at the Milford City, Utah FORGE Site”. This research made use of the resources of the High-Performance Computing Center at Idaho National Laboratory, which is supported by the Office of Nuclear Energy of the U.S. Department of Energy and the Nuclear Science User Facilities under Contract No. DE-AC07-05ID14517. Any opinions, findings, and conclusions, or recommendations expressed in this material are those of the authors and do not necessarily reflect those of the DOE or the U.S. Government.

REFERENCES

Finnila, A.: Utah FORGE: Updated Discrete Fracture Network Model for the FORGE Site - 2025. United States. (2025). https://doi.org/10.15121/2476297. https://gdr.openei.org/submissions/1685.

Finnila, A.: Identification of Fracture Flow Pathways at Utah FORGE. Proceedings of the 51st Workshop on Geothermal Reservoir Engineering, Stanford University, Stanford, California, (2026). (SGP-TR-230).

Giudicelli, G., et al.: MOOSE 3.0: Enabling massively parallel multiphysics simulation. SoftwareX, 25 (2024). https://doi.org/10.1016/j.softx.2023.101616

Hartvig, S., Huseby, O., Fredd, C., & Giri, P.: Utah FORGE: RESMAN Well 16A(78)-32 and 16B(78)-32 Stimulation and Circulation Tracer Test Results - 2024. [Data set]. Geothermal Data Repository. RESMAN Energy Technology. (2025). https://doi.org/10.15121/2507444

Jones, C., McLennan, J., & Moore, J.: Characterization of Drill Core from Stimulated Crystalline Rock Following Hydraulic Fracturing at the Utah FORGE Geothermal Test Site. Proceedings of the 50th Workshop on Geothermal Reservoir Engineering, Stanford University, Stanford, CA (2025).

Liu, R., Podgorney, R., Finnila, A., Xing, P., McLennan, J., & Moore, J.: Development of a Coupled Multi-Field Utah FORGE Native State Model: Phase 3 Update. In 2022 Geothermal Rising Conference: Using the Earth to Save the Earth, GRC 2022 (pp. 589-596). Geothermal Resources Council, (2022).

McLennan, J., England, K., & Swearingen, L.: Utah FORGE: Wells 16A(78)-32 and 16B(78)-32 Extended Circulation Test Data - August and September 2024. United States. (2024). https://doi.org/10.15121/2475065. https://gdr.openei.org/submissions/1683.

Moore, J., Podgorney, R., Pankow, K., Simmons, S., McLennan, J., Wannamaker, P., Wendt, D., Mattson, E., & Wickstrom, L.: The Utah FORGE Site: Characterization of Regional Geologic Structure. Proceedings of the 44th Workshop on Geothermal Reservoir Engineering, Stanford University, Stanford, California, (2019). (SGP-TR-214).

Otchere, C., Munday, L., Dhulipala, S., Shields, M., Podgorney, R., & Rao, K.: Using multi-objective Bayesian optimization to calibrate fracture and matrix properties to Utah FORGE circulation data. (To be submitted), (2026).

Podgorney, R., Finnila, A., Simmons, S., & McLennan, J.: A reference thermal-hydrologic-mechanical native state model of the Utah FORGE enhanced geothermal site. Energies, 14(16), 4758, (2021).

Wilkins, A., Green, C.P., & Ennis-King, J.: An open-source multiphysics simulation code for coupled problems in porous media. Computers & Geosciences, 154, 104820 (2021). https://doi.org/10.1016/j.cageo.2021.104820